This work was carried out in whole or in part within the framework of the NOMATEN Center of Excellence, supported from the European Union Horizon 2020 research and innovation programme (Grant Agreement No. 857470), the European Regional Development Fund via the Foundation for Polish Science International Research Agenda PLUS programme (Grant No. MAB PLUS/2018/8), *and the initiative of the Ministry of Science and Higher Education 'Support for the activities of Centers of Excellence established in Poland under the Horizon 2020 program' under agreement No. MEiN/2023/DIR/3795.*

This is the accepted manuscript submitted to: Diamond and Related Materials Volume 147, August 2024, 111336, published on 29 June 2024 with the embargo period till: 29 June 2026.

DOI: 10.1016/j.diamond.2024.111336

Computational modeling of CH_4 and CO_2 Adsorption on Monolayer Graphenylene: Implications for Optoelectronic Properties and Hydrogen Production

A. Aligayev[a,b], F. J. Dominguez-Gutierrez[b,c], M. Chourashiya[b,d,e], S. Papanikolaou[b], Q. Huang[a]

[a] *Hefei Institutes of Physical Science, Chinese Academy of Science, University of Science and Technology of China, Hefei, 230026, China*
[b] *NOMATEN Centre of Excellence, National Centre for Nuclear Research, ul. A. Sołtana 7, 05-400 Otwock, Poland*
[c] *Institute for Advanced Computational Science Stony Brook University Stony Brook, NY 11749, USA*
[d] *Guangdong Technion Israel Institute of Technology, Shantou, 515063, China*
[e] *Technion, Israel Institute of Technology, Haifa, 32000, Israel*

Abstract

Graphenylene (GP) is a two–dimensional carbon allotrope with a hexagonal lattice structure containing periodic pores. The unique arrangement of GP offers potential applications in electronics, optoelectronics, energy storage, and gas separation. Specifically, its advantageous electronic and optical properties, make it a promising candidate for hydrogen production and advanced electronic devices. In this study, we employ a computational chemistry–based modeling approach to investigate the adsorption mechanisms of CH_4 and CO_2 on monolayer GP, with a specific focus on their effects on optical adsorption and electrical transport properties at room temperature. To simulate the adsorption dynamics as closely as possible to experimental conditions, we utilize the self–consistent charge tight–binding density functional theory (SCC–DFTB). Through semi–classical molecular dynamics (MD) simulations, we observe the formation of H_2 molecules from the dissociation of CH_4 and the formation of CO+O species from carbon dioxide molecules. This provides insights into the adsorption and dispersion mechanisms of CH_4 and CO_2 on GP. Furthermore, we explore the impact of molecular adsorption on optical absorption properties. Our results demonstrate that CH_4 and CH_2 affects drastically the optical adsorption of GP, while CO_2 does not significantly affect the optical properties of the two–dimensional material. To analyze electron transport, we employ the open–boundary non–equilibrium Green's function method. By studying the conductivity of GP and graphene under voltage bias up to 300 mV, we gain valuable insights into the electrical transport properties of GP under optical absorption conditions. The findings from our computational modeling approach might contribute to a deeper understanding of the potential applications of GP in hydrogen production and advanced electronic devices.

1. Introduction

Energy plays a vital role in human survival and advancement. Currently, our main energy supply heavily depends on fossil fuels such as coal, oil, and natural gas. However, the excessive use of these fuels has caused their depletion. Increasing the uptake of renewable energy could play a crucial role in assisting the world in reaching vital climate targets by 2050 [1]. Hydrogen (H_2) energy emerges as a plentiful, eco–friendly, low–carbon alternative [2]. It can be sourced from various outlets, renewable and non–renewable alike [3]. The primary techniques for generating H_2 from methane encompass steam reforming, dry reforming, partial oxidation, and catalytic decomposition of methane.

Detecting H_2 poses challenges due to its colorless and odorless nature, especially at low concentrations [4]. Consequently, the development of highly sensitive H_2 gas sensors is vital for effective monitoring in production, transportation, storage, and usage scenarios. Sensors detect gases through the physical adsorption of gas molecules onto a surface. These sensors use a gas–sensitive material, such as carbon–based ones, that change their properties upon gas adsorption, offering high sensitivity and selectivity [5]. The high sensitivity of graphene to the local environment has shown to be highly advantageous in sensing applications, where ultralow con-

centrations of adsorbed molecules induce a significant response to the electronic properties of graphene [6, 7, 8, 9, 10, 11]. Additionally, carbon–based materials can be tailored by varying their surface chemistry, porosity, and morphology. The hybridization of carbon atoms into sp–, sp^2–, and sp^3–orbitals can create diverse carbon allotropes exhibiting distinct dimensionalities [12, 13]. Ongoing research focuses on improving the performance and reliability of gas adsorption sensors and exploring new materials and sensing mechanisms for enhanced gas sensing capabilities [14, 15, 16, 17, 18, 19].

Graphenylene (GP), an intriguing carbon allotrope sharing the same point group (D_{6h}) as graphene, is composed of sp^2–hybridized carbon atoms arranged in hexatomic and tetratomic rings [20, 21, 22, 23]. Qi-Shi Du et al. successfully synthesized layers of graphenylene, also referred to as biphenylene–carbon (BPC), by dehydrating and polymerizing 1,3, 5–trihydroxybenzene [24, 25]. The process involved the removal of three water molecules from a 1,3,5–trihydroxybenzene molecule using dehydrant aluminum oxide, leading to the amalgamation of bare 6C rings (benzynes) and the formation of a small segment of the 2D carbon crystal. Furthermore, polymerization could also take place through intermolecular dehydration between 1,3,5– trihydroxybenzene molecules, where the fragments of the 2D carbon crystal grew rapidly. The experimental construction of GP involved utilizing planar 4-carbon rings and 6-carbon rings with sp^2 electron configuration, experiencing slight distortions that ultimately resulted in the formation of a large planar conjugated π-system [26]. It possesses a hexagonal lattice structure with periodic pores, offering a high surface area and pore volume. These characteristics make GP a promising material for gas adsorption and separation applications. The unique topology of GP allows for selective adsorption of specific gas molecules, making it a potential candidate for highly efficient and selective gas separation and storage processes [27, 28, 29]. The identification of hollow adsorption sites in GP is of great interest, as these sites hold significant potential for various applications, including gas separation [30, 31, 32, 33]. These features also motivated researchers to study more advanced materials, inorganic graphenylene (IGP) family [34, 35, 36, 37], such as IGP based on boron nitride [38], IGP-ZnO [39], IGP-GaN [40], IGP-SiC [41], and so on. The authors proposed for the first time inorganic graphenylene based on indium nitride (IGP-InN). The electronic, mechanical, structural, and vibrational properties, as well as strain effects, showed the potential of this new 2D material [35, 37]. It is also delved into the structural and electronic properties of inorganic graphenylene–like germanium carbide (IGP–GeC), investigating mechanical deformations under strain through computational simulations using DFT [36].

The growing importance of air quality and safety has created a demand for advanced gas sensors. Porous carbon–based materials have emerged as promising candidates for such sensors due to their comparable electronic mobility and mechanical properties to graphene. Additionally, these materials offer the added advantage of enabling the dispersion of single atoms within acetylenic pores. Building upon the research progress in graphene, investigations into post–graphene 2D carbon–based materials have swiftly demonstrated diverse electronic devices and emerging charge transport phenomena. However, despite the growing understanding of electronic transport in individual 2D materials, practical wafer–scale implementation faces significant challenges [42, 43]. Therefore, the development of reliable techniques for wafer–scale growth, ensuring uniformity and predictable thickness poses considerable hurdles from a materials science perspective. Thus, carbon materials exhibit versatile bonding abilities, ranging from sp^1 to sp^3 hybridization, and encompass a variety of allotropes, including fullerene, graphite, diamond, graphene, carbon nanotubes, and fibers [44, 45, 46]. Porous carbons can be obtained through the carbonization of natural or synthetic precursors, followed by activation, allowing for approximately adjustable pore sizes ranging from micropores (< 2 nm) to mesopores (2-50 nm) and macropores (> 50 nm). Diverse synthesis strategies, such as template methods, etching of metal carbides, and sol–gel processing, have been explored to create porous carbon materials with controlled pore structures at both the micropore and mesopore levels [44].

GP, with its exceptional porous architecture and remarkable electronic features hold great promise as a material for the development of high–performance molecular gas sensors. In order to save financial resources and avoid exhaustive experimental trials, detailed atomistic simulations are essential to complement practical exploration. The Self– Consistent–Charge Density– Functional Tight– Binding (SCC–DFTB) method [47, 48] is employed in this study to

investigate the potential applications of GP in the detection of important molecular gases such as CH_4 and CO_2 and their species, which have significant environmental implications [49, 50]. Here, the study examines hydrogen production through methane dissociation and CO_2 reduction mechanisms, emitting CH_4 and CO_2 molecules with impact energies near their dissociation energies and analyzing their interactions with GP. Additionally, the results are compared with those obtained for graphene. Further computational research that closely emulates dynamic mechanisms observed in experiments is necessary to fully explore the potential of graphenylene, including its effects on optical absorption, electron transport performance, and enhancement of material sensitivity. Our primary objective is to contribute to the characterization of GP as a promising material for future research and the development of materials for ultrafast gas sensors and gas separation applications.

2. Computational Methods

The SCC–DFTB method is a computational approach that approximates traditional Density Functional Theory (DFT) by considering valence electron interactions in MD simulations. It serves as a valuable tool for accurately predicting structures and thermodynamic properties prior to synthesis, providing insights into the gas adsorption properties of 2D carbon–based materials and their potential applications in various gas adsorption environments. The SCC–DFTB method involves solving Kohn–Sham equations to obtain total valence electronic densities and energies for each atom utilizing a Hamiltonian functional based on a two-center approximation and optimized pseudo–atomic orbitals as the basis functions [47, 48]. Slater–Koster (SK) parameter files are utilized to provide tabulated Hamiltonian matrix elements, overlap integrals, and repulsive splines fitted to DFT dissociation curves. These parameters describe the overlap and hopping integrals between pairs of atoms in the tight–binding Hamiltonian. The optimal set of Slater-–Koster parameters have two main requirements: a good reproduction of the structure of the relevant electronic bands, and faithful representation of the orbital contribution along such bands. Therefore, in the scope of this approach the total energy of the system is expressed as

$$E^{\mathrm{DFTB}} = E_{\mathrm{band}} + E_{\mathrm{rep}} + E_{\mathrm{SCC}}, \qquad (1)$$

with the band structure energy, E_{band}, defined from the summation of the orbital energies ϵ_i over all occupied orbitals Ψ_i; the repulsive energy E_{rep} for the core–core interactions related to the exchange– correlation energy and other contributions in the form of a set of distance–dependent pairwise terms; and an SCC contribution, E_{SCC}, as the contributions given by charge–charge interactions in the system. Therefore, the electronic energy is calculated by summing the occupied Kohn-Sham (KS) single–particle energies and the contributions from repulsive energies between diatomic atoms. To account for self–consistent charge (SCC) effects during the dynamics, an iterative procedure is used.

To validate our findings, density functional theory (DFT) calculations were conducted using the PBE exchange–correlation functional. The calculations were carried out under periodic boundary conditions, and the Brillouin zone integration was performed with the Γ point considered. Kohn–Sham orbitals were employed as plane waves up to an energy cutoff of 90 Ry to ensure convergence in the structural properties of the systems. The Quantum-ESPRESSO ab–initio package with relativistic- corrected pseudo-potentials was utilized for computing the density of states, system energies, and band structures. The total electronic density of states (DOS) for GP reveals significant overlaps between the C–2s and C–2p curves, indicating the presence of strong sp^3 hybridized covalent bonding states.

2.1. Structures and binding energies

GP is a two–dimensional carbon allotrope that possesses a hexagonal lattice structure with periodic pores and its structure as reported by Balaban et al. [20] and Martins et al. [28], consists of three types of symmetrically distributed rings: dodecagon (C_{12}), hexagon (C_6), and square (C_4), which forms a tiling of the Euclidean plane. The unit cell of GP, determined by Fabris et al. using DFT[51, 34], belongs to the $P6/mmm$ space group and contains a single irreducible atom, which is considered in our SCC–DFTB calculations. In this study, optimization of the GP unit cell was conducted, resulting in lattice parameters of $\vec{a} = \vec{b} = 6.735$ Å and bond lengths of 1.50 Å for the square ring and 1.48 Å for the hexagon ring identifying seven points of high symmetry [41]. Periodic boundary conditions were applied in the x–y directions to simulate a semi-infinite surface. For the k–point sampling, a $4\times4\times1$ Monkhorst–Pack set was

employed throughout all calculations. These findings align well with experimental measurements indicating 1.42–1.46 Å for the 6–C rings and 1.50–1.52 Å for the two bonds joining the 6–C rings [24, 37], as illustrated in Fig. 1a). The central nanopore (dodecagon ring) in the unit cell has a diameter of 5.66 Å, in good agreement with DFT data [51, 22] and experimental measure of 5.8 Å [24]. To compare the adsorption capabilities of GP with graphene, the unit cell of graphene was optimized using well–known lattice parameters and bond lengths, as depicted in Fig. 1b). Periodicity on $x-y$ plane was considered with a k–point sampling of 12×12×1 Monkhorst– Pack set for all the calculations.

The interaction potentials between H_2, CO_2, and CH_4 molecules with graphene and GP are investigated using the DFTB method. To avoid interactions with periodic replicas, the unit cell of the optimized GP structure is replicated by 3×4×1 and the unit cell of graphene is replicated by 5×5×1 along the x and y directions. The larger cells are initially optimized using SCC-DFTB. Adiabatic calculations follow to determine potential energy curves. These curves depict molecule interactions with fully relaxed periodic

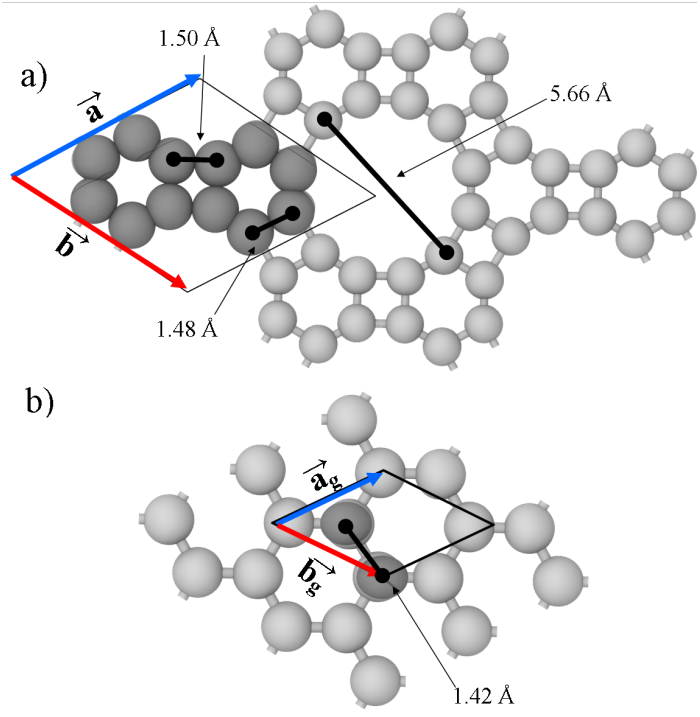

Figure 1: (Color online). Optimized structures of graphenylene (a) and graphene (b) were obtained using the SCC–DFTB method. The calculated bond lengths and lattice parameters are in good agreement with the reported DFT data [51].

sheets at different distances and adsorbate sites, incorporating dispersion corrections to better account for the long-range dispersion forces are done through van der Waals interactions between carbon atoms and molecules. [52, 53]. Thus, the total energies, $E(z)$, of the molecule–2D material system with a separation z between the adsorbate sites and the center of mass of the molecules are varied above the surface in a range of 0.5 to 7 Å, which defines the computation of the adsorption potential as a function of the distance separation. The total energy is then computed as:

$$E(z) = E_{\text{Tot}} - (E_{\text{2Dmaterial}} + E_{\text{Molecule}}), \qquad (2)$$

where E_{Surface} is the total energy of the 2D material; E_{Molecule} is the total energy of the isolated molecule: H_2, CH_4, and CO_2; and E_{Tot} is the energy of the interacting system at every z–distance. Thus, the binding energy is defined as $E_b = E(z_{\text{min}})$ with z_{min} as the equilibrium molecule–surface distance. Total energy calculations are performed for the molecule–2D material system, varying the distance between the surface and the center of mass of the molecules along the z–axis. Three different adsorption sites for graphene and 5 sites for GP are considered based on unit cells of the materials. The molecular symmetry planes are consider with respect to the surface plane in the calculations. The repulsive potential is cut off at a distance below the second nearest–neighbor interaction region for numerical stability.

2.2. Semi–Classical Molecular Dynamics Simulations

The adsorption dynamics of H_2, CH_4, and CO_2 molecules on graphene and GP were investigated using semi-classical molecular dynamics simulations. For graphene, a $5\times5\times1$ supercell was used, while for GP, a $3\times3\times1$ supercell was employed. The surfaces were optimized and equilibrated to a temperature of 300 K using a Nose–Hoover thermostat. To simulate the adsorption dynamics, a target area of 1 nm^2 on the surface was defined, and molecules were randomly distributed on a parallel plane to the surface by using the velocity Verlet algorithm. The impact energy of the molecules was 8 eV, and 650 MD simulations with independent trajectories were performed for each molecule. A time step of 0.25 fs was used, and the molecules were emitted vertically with random orientations at an initial distance of 0.6 nm above the surface. Each MD simulation is performed for a duration of 350 fs, this time–frame was meticulously

chosen to ensure convergence in our MD simulations. It provided ample time for the molecules to travel away from the carbon sheets while also guaranteeing that the attached molecules remained bonded to the carbon atoms, preventing any detachment from the sheets. We have previously employed this approach to study hydrogenation mechanisms of fullerene cages [54], electronic properties of borophene [55], and dynamic physisorption pathways of molecules on alumina surfaces [56], demonstrating excellent agreement with first principles DFT calculations.

After conducting MD simulations at room temperature and an impact energy of 8 eV, the emission of hundreds of H_2, CO_2, and CH_4 molecules is analyzed by calculating the probabilities of adsorption, reflection, and transmission, which are defined as:

$$P = 100 \times \frac{N_x}{N_{\text{Tot}}}, \tag{3}$$

where N_{Tot} is the total number of MD simulations, while N_x is the number of cases for adsorption, reflection, and transmission calculated by using the following conditions based on the last frame of the MD simulations: 1) Adsorbed cases: Molecules with a final position between a sphere centered at the material with a radius of 3.5 Å and the direction of the velocity vector points towards the surface is considered as adsorbed; 2) Reflection cases: Molecules with a final position larger than 3.5 Å and a velocity vector oriented in the opposite direction to the surface normal is counted as reflected; 3) Transmission cases: Molecules with a final position below the surface and a distance larger than -3.5 Å are counted as transmitted.

2.3. Optical absorbance and electron transport calculations

The optical absorption is investigated within the DFTB framework as an electronic dynamic process in response to an external electric field [57, 58]. The conventional adiabatic approximation gives the time evolution of the electron density matrix by time integration of the Liouville–von Newmann equation expressed as

$$i\hbar\frac{\partial\hat{\rho}}{\partial t} = S^{-1}\hat{H}\hat{\rho} - \hat{\rho}S^{-1}, \tag{4}$$

where $\hat{\rho}$ is the single electron density matrix, $\hat{S}$ is the overlap matrix, and $\hat{H}$ is the system Hamiltonian that includes the external electric field as $\hat{H} = \hat{H}_0 + E_0\delta(t - t_0)\hat{e}$ with E_0, the magnitude of the electric field, and $\hat{e}$, its direction. Under the framework of linear response, the absorbance $I(\omega)$ is calculated as the imaginary part of the Fourier transform of the induced dipole moment caused by an external field. In this study, the external field strength was set to $E_0 = 0.001$ V/Å. The induced dipole moment was evaluated over a 200 fs time period using a time step of $\Delta t = 0.01$ fs. The Fourier transform was performed with an exponential damping function (using a 5 fs damping constant) to eliminate noise.

The Non–Equilibrium Green's Functions formalism (NEGF) is a robust theoretical framework commonly used for modeling electron transport in nano–scale devices and is implemented in the DFTB code [59]. In Fig. 2, a detailed illustration is presented of the geometric configuration of the graphene and GP structures, highlighting the specific regions involved in the electron transport calculations. To ensure accurate and reliable results, several steps are followed: 1) The structures are carefully divided into distinct sections, including the principal layers, two electrode contacts (drain and source), and the device

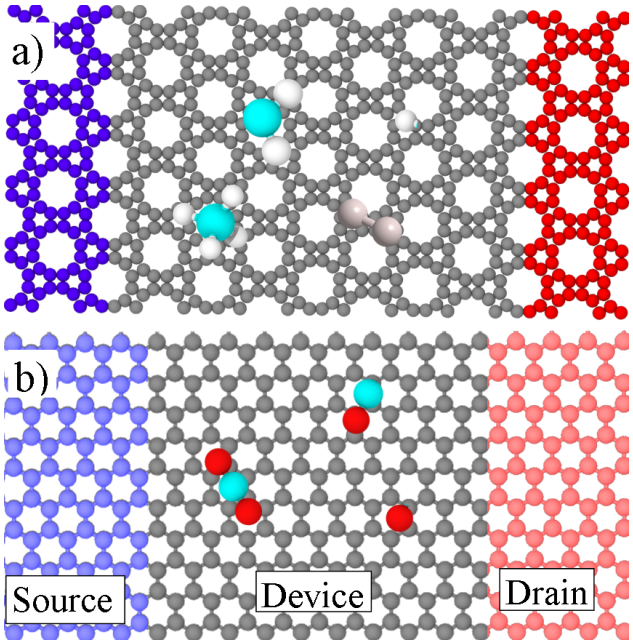

Figure 2: Optimized structures employed in the electron transport calculations. In (a), the structure is shown for graphenylene with CH_4, CH_2, and H_2 molecules and a hydrogen atom attached, while in (b), graphene sheet is depicted with CO_2 and CO molecules with an oxygen atom. The blue and red regions represent the two principal layers. The middle region corresponds to the device under investigation and the size of the molecules is increased for better visualization.

region. This partitioning enables a systematic analysis of electron transport within the designated "scattering region."; 2) The drain section, represented by red spheres, corresponds to the region where electrons exit the device, while the source section, depicted by blue spheres, represents the region where electrons enter the device; 3) To simulate realistic conditions and investigate the impact of specific molecules on electron transport, CO_2 molecules are introduced into the graphene device section, and CH_4 molecules are added to the GP device section. This allows us to study the interaction between the adsorbates and the carbon-based materials and observe their influence on the electron transport properties; and 4) Before performing the electron transport calculations, the entire system undergoes an optimization process. This optimization involves adjusting the positions and orientations of the atoms to find the most energetically favorable configuration for the combined graphene/GP–adsorbate system.

3. Results

In Fig. 3 we present DFTB calculations revealing that GP possesses a bandgap of approximately 0.96 eV from the DOS calculations, while graphene lacks a bandgap altogether. The electronic band structures also show that the valence and conductance bands for carbon atoms are located at the Γ point. The band gap of GP is structure–dependent and can range from zero to a few electron volts, as theoretical studies have predicted band gaps for GP ranging from 0 eV to approximately 3.3 eV; depending on the specific structure and calculation method employed [6, 26]. It should be noted that the semi–local functionals tend to underestimate the band gaps of GP structures. It is also noticed the selected path show the characteristic gaps at the M and Γ point reported by DFT calculations [22]. The slight discrepancy in negative energies can be attributed to variations in the SK parameters used in our calculations, which are based on the MIO (minimalist iterative orthogonalization) approach. In this method, the electronic structure of our system is approximated by considering only a minimal set of atomic orbitals, leading to significant computational savings compared to our DFT calculations. However, it is important to note that this approach is inherently less accurate than full DFT calculations, as it relies on semi–empirical parameterizations and simplified electronic structure models. These simplified models may not capture the full complexity of the system accurately. Nevertheless, the fair agreement observed still provides validation for our results.

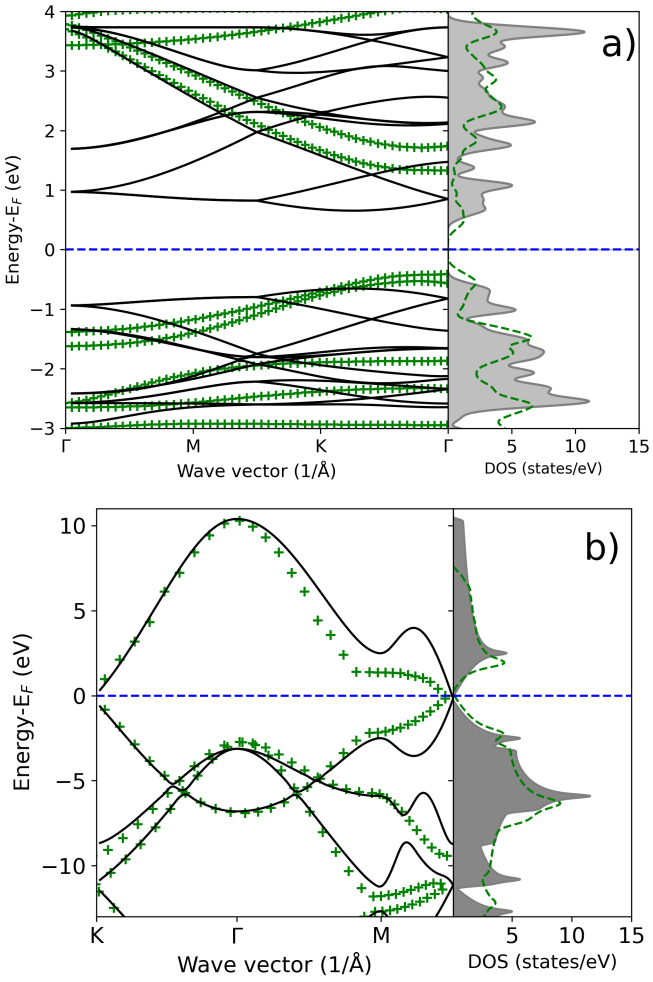

Figure 3: Band structure and density of states for GP in a) and for graphene in b). Similarities are observed due to the hexagonal arrangement in the unit cell of the materialsi. DFT calculations are represented by dashed lines for the density of states (DOS) and marked with cross-points for the band structure.

Fig. 4 present results for the physisorption pathways for H_2, CH_4, and CO_2 molecules on both graphene and GP sheets. In the case of graphene, the bond length for molecular hydrogen and methane molecules is observed to be approximately 2.2 Å, with binding energies of -0.052 eV (in good agreement with Lee et al. [60]) and -0.165 eV, respectively. Meanwhile, the carbon dioxide molecule exhibits a bond length of 2.6 Å and a binding energy of -0.151 eV. For GP, it is found that H_2 and CH_4 molecules exhibit bond lengths of 2.25 Å, along with binding energies of -

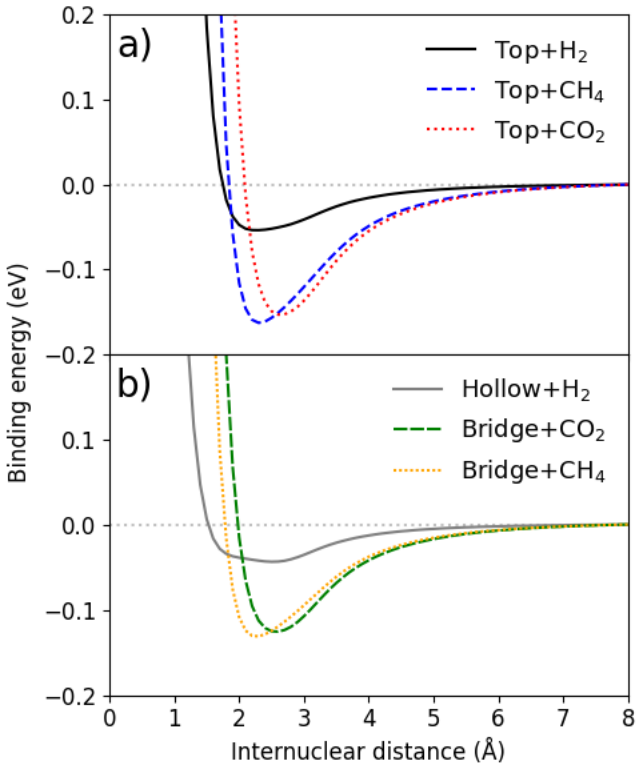

Figure 4: Binding energies are presented as a function of separation distance for both graphene (a) and graphenelyne (b), showcasing the lowest energy states and the impact of distinct adsorbate sites on the binding of H_2, CO_2, and CH_4 molecules. The analysis reveals a stronger tendency for adsorbate molecules to form bonds with the top carbon atoms in graphene, while graphenelyne displays diverse adsorbate sites due to its sp hybridization. The remaining potential energy curves (PECs) can be found in the Supplementary Material accompanying this manuscript.

0.043 eV and -0.132 eV, respectively. CO_2 on GP has a bond length of 2.62 Å, accompanied by a binding energy of -0.125 eV. In the SM, we present the physisorption pathways of all the adsorbate site of both carbon sheets, showing that adsorbate sites associated with the hexagonal and square holes exhibit a lower likelihood for molecule adsorption; specially methane molecules are more likely to bond to the top of the carbon atoms, with a binding energy of -0.2 ± 0.05 eV showing excellent conditions for gas separation for this energy barrier [22, 29]. During the calculations, we did not observe significant structural deformation of the GP sheets, except for slight bending at the points where bond energy is minimum.

These results serve as the basis for configuring the initial conditions in our MD simulations. To ensure an initial distance greater than 8 Å, interactions between the molecules and the carbon sheet are prevented at the outset of the simulation. These findings offer valuable insights into the interactions between carbon sheets and these molecules, which are essential for understanding the physical processes in our MD simulations. It is worth noting that dispersion corrections play a significant role in these calculations, particularly due to the hybridization of the system and the presence of CH_4 molecules. Similar trends are observed for graphene, where the adsorbate site located at the top of the carbon atoms is more favorable for both physisorption and chemisorption mechanisms confirming reported results for hydrogen trapping by graphene [53], indicating a higher likelihood of attracting molecules.

3.1. Dynamical adsorbtion of CH_4 and CO_2 molecules

In Table 1 we present the probabilities of transmission, adsorption, and reflection for both carbon surfaces and different molecular projectiles. For graphene, the dissociation of H_2 and CO_2 molecules among the reflected molecules was not observed. The molecule initiates its trajectory with a kinetic energy (KE) of 8eV. However, it undergoes a gradual deceleration as it comes into contact with the carbon atoms. Upon colliding with a carbon sheet at various adsorbate sites, the molecule is reflected, promoting its vibrational and rotational movements. To observe dissociation mechanism, a higher impact energy than 10 eV would be required. However, it is worth noting that such high–energy collisions could result in the creation of vacancies in the graphene sheet by displacing a carbon atom, which is not observed in our MD simulations at 8 eV. On the other hand, some of the reflected CH_4 molecules underwent dissociation, and a few of them were able to attach to the graphene sheet. In order to bond more CH_2 molecules to graphene, a lower impact energy would be sufficient. In the case of GP, its inherent porosity allowed for a higher number

	Graphene			Graphelyne		
Probability	H_2	CO_2	CH_4	H_2	CO_2	CH_4
Transmission	0	0	0	5.28	1.28	49.12
Adsorption	0	0	16.8	0	9.66	1.60
Reflection	100	100	83.2	94.72	89.06	49.28

Table 1: probabilities of different cases observed in the MD simulations, including transmission, reflection, and adsorption, for both graphene and GP. The results clearly demonstrate that GP exhibits superior performance as a material for gas separation compared to graphene.

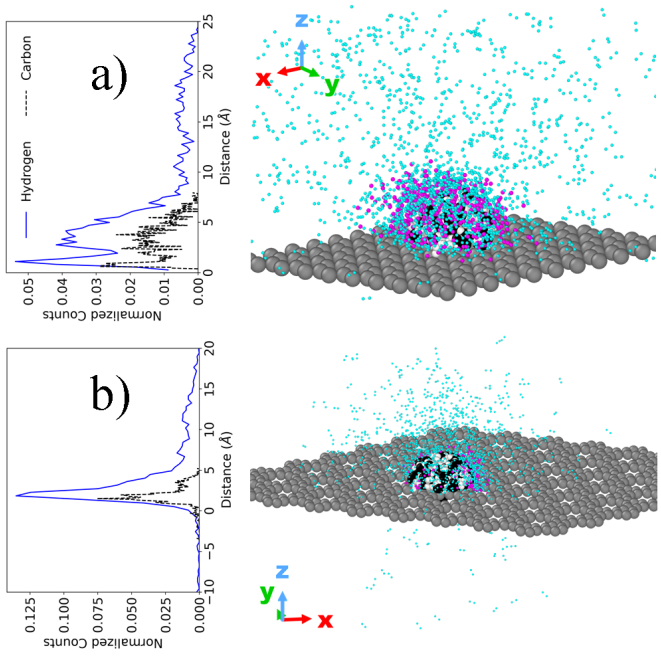

Figure 5: The visualization of the final frame in each MD simulation simultaneously enables a thorough analysis of the adsorbed, reflected, and transmitted cases for both graphene (a) and graphenelyne (b); with their corresponding histogram for the distance counts on the z-axis. The structures consist of carbon atoms depicted as gray spheres. Adsorbed CH_2 molecules are represented by black spheres for carbon atoms and white spheres for hydrogen atoms. Reflected molecules are shown as turquoise spheres representing molecular hydrogen, and purple spheres representing carbon atoms.

of transmitted cases for both H_2 and CO_2 molecules. We observed that some carbon dioxide molecules dissociated into CO+O, with the CO molecules bonding to the GP sheet. This highlights the advantage of GP's porous structure in facilitating gas transmission and reactivity compared to graphene.

From the MD simulation results, it becomes apparent that CH_4 molecules can undergo reflection and dissociation, leading to the formation of CH_2 and H_2 as the main process. Figure 5 displays a histogram of the counts of the final positions of the C and H atoms for the final frames of the simulations for graphene (a) and GP (b), providing a visual representation of the observed dynamics. This plot is used to count for the number of events with a probability of transmission, reflection, or absorption. Within our observations, it is found that CH_2 molecules are more likely to bind to the carbon sheets. In alternative scenarios, both CH_2 and H_2 molecules are seen to dissociate after collision with the carbon sheets. A notable observation is the differential behavior of hydrogen molecules in graphene compared to GP.

The GP's porous structure facilitates the transmission of hydrogen molecules, making it a promising candidate for applications such as hydrogen production in the context of energy generation. While graphene sheets present high scattering of H_2 molecules. We have found that CH_4 molecules are unable to transmit through graphene, whereas in the case of GP, there is a probability of approximately 50% for transmission, accompanied by dissociation and the production of molecular hydrogen. This behavior can be attributed to the porous nature of the materials and the impact energy of the emitted. Additionally, the velocity distributions of carbon (C), oxygen (O), and hydrogen (H) atoms at the last frame are analyzed considering all the MD simulations for each case. Notably, molecular hydrogen exhibits the highest velocities, while CH_2 molecules exhibit the lowest velocities after being reflected by the carbon sheets. This observation provides an initial indication of the bonding behavior of the ejected molecules, which is discussed in more detail within the SM.

Furthermore, it has been noted that CH_2 molecules can form bonds with GP by infiltrating the porous structure and binding to the underlying C atoms. This property distinguishes GP from graphene, as the latter typically requires the presence of defects to enable molecule transmission. Here, the distinctive arrangement of sp^2–carbon atoms in GP creates a two–dimensional lattice with regularly spaced sized pores which is notably larger than the kinetic diameters of H_2, CO_2, and CH_4, facilitating the favorable diffusion of these molecules. This mechanism highlights the potential of GP is a promising material for gas separation, particularly for CH_4, as supported by our MD simulations for CO_2 purification as well.

Figure 6 presents the analysis of reflected molecules from the surfaces of graphene and GP at an impact energy of 8 eV. The analysis involves determining the internuclear distance between atoms in the final frame of the simulations. In the case of H_2 molecules (Figure 6a), it is observed a uniform distribution of the internuclear distance around the bond length of 0.74 Å. This distribution arises from the excitation of vibrational and rotational states due to the exchange of kinetic energy during a collision with the surfaces, as previously discussed. For CO_2 molecules, the splitting of the molecules into CO and O is evident, with a majority exhibiting a homogeneous distribution around 1.43 Å for the internuclear distance

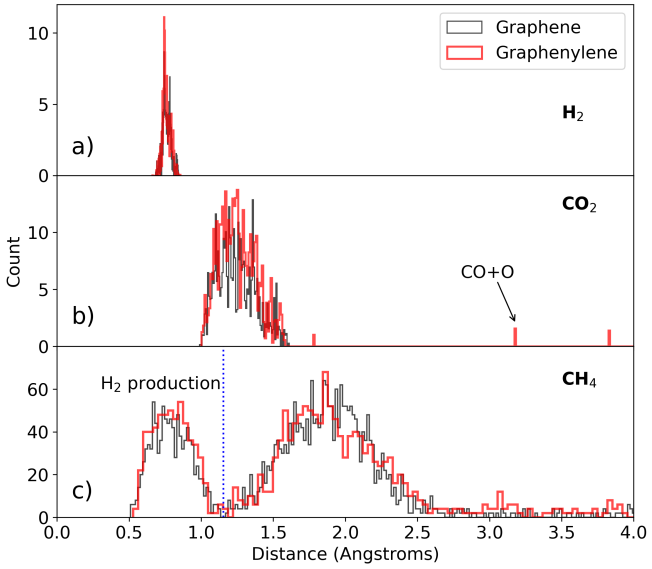

Figure 6: Analysis of reflected molecules from graphene and graphenylene surfaces. Upon collision, H_2 molecules are reflected without breaking their bonds, but changing their angular momentum. Most of the CO_2 molecules are reflected, while a fraction of them undergo dissociation into CO and O. Interestingly, the collision with the surfaces results in the production of H_2 for the majority of CH_4 molecules.

which corresponds to the CO bond length. Oxygen atoms are identified with an internuclear distance larger than 2.5 Å. Finally, CH_4 molecules undergo splitting into CH_2 and H_2 molecules with the highest probabilities, with CH_3+H dissociation with a low probability. Molecular hydrogen is characterized by an internuclear distance of around 0.74 Å and a higher degree of excitation in vibrational states. The main dissociation channel is identified as CH_2 (methylene) molecules, with a peak observed in the histogram at approximately 1.8 Å, representing the internuclear distance between H atoms. The porosity of GP makes it a more promising candidate for H_2 production compared to graphene, as demonstrated by MD simulations. The histogram illustrates the distribution of reflected molecules with different bond lengths corresponding to their excited vibrational states. For instance, when H_2 molecules are emitted onto the 2D materials, they tend to vibrate towards states close to their ground state. On the other hand, H_2 molecules originating from the dissociated methane exhibit various bond lengths due to their excited vibrational and rotational states. This concept also applies to CO_x and CH_x molecules.

3.2. Optical Absorption Spectra, electron transport and sensitivity

Before performing the optical absorption calculations, unconstrained optimizations of the carbon sheet were conducted in the presence of various molecules and atoms, each in different scenarios. In instances where a physisorption pathway was relevant, constrained optimization calculations were performed to establish the optimal bond lengths. This approach was adopted to simplify the computational process, allowing for a more efficient and accurate determination of the atomic configurations.

The optical spectra are calculated for different cases of molecular adsorption: 1) In the analysis of hydrogen molecules, consideration was given to a single H_2 molecule positioned above a carbon atom, along with two hydrogen atoms located above two distinct carbon atoms, where the interaction between them is minimal and the obtained results are in a good agreement with experimental and ab–initio data regarding the absorption intensities of the interband transitions occurring in the Dirac band (mid-IR and visible) [61, 46, 62]. In the context of the CO_2 and its split CO+O counterpart, the CO_2 molecule was initially positioned above a carbon atom, followed by its placement on two different carbon atoms in the resulting CO+O system. The effect of carbon dioxide on the graphene sheet is similar to that observed for the H_2 molecule. For GP, the influence decreases compared to the pristine case. However, the split of CO+O enhances the absorbance of the graphene sheet at the same wavelength as the CO_2 molecule. For the GP case, the absorbance rate is lower than that observed in the carbon dioxide case. 3) For methane molecules, several configurations is investigated: CH_4, CH_2+H_2 (molecular hydrogen and methylene as a main dissociation channel), CH_2+H+H, and CH_2, as they are crucial for sensor development [63, 31].

Figure 7 presents the normalized optical absorption spectrum of graphene (a) and GP (b) obtained using the Liouville–von Neumann equation for the hydrogen molecule, methane, and carbon dioxide and the rest of the results are displayed in the SM. These findings reveal that pristine graphene doesn't interact with visible light, as expected [64]. However, when it's paired with a hydrogen molecule or carbon dioxide, graphene becomes more effective at absorbing visible light. In contrast, the addition of a methane molecule primarily enhances its ultraviolet absorption capabilities. Furthermore, when it comes to the GP,

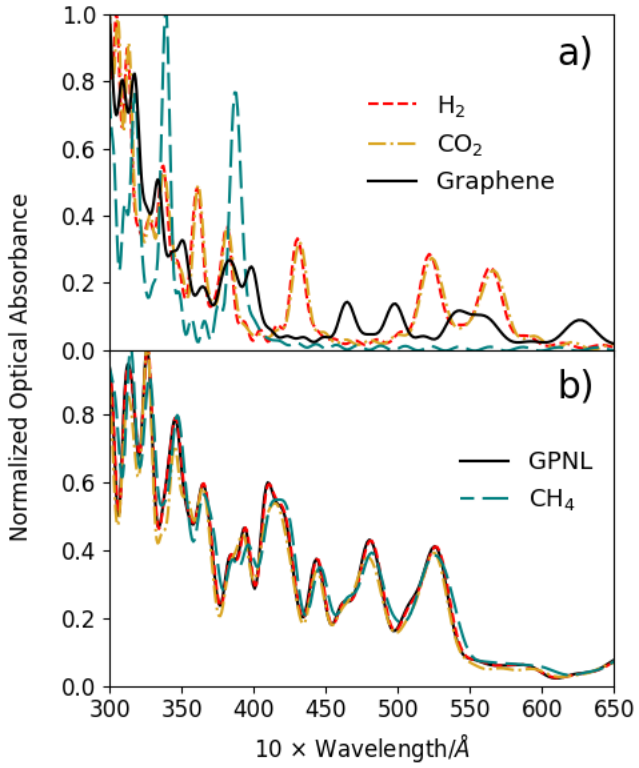

Figure 7: Optical absorbance spectra of graphene (a) and graphenelyne (b) in the visible range, considering H_2, CO_2, and CH_4 molecules adsorbed by the surfaces. The presence of split CH_4 molecules significantly impacts both surfaces.

the presence of attached molecules doesn't exert any discernible effect on the optical properties of the carbon sheet. The structural characteristics of the pores do not significantly enhance light absorption, and its band gap doesn't cause excessive scattering of visible light. This underscores the material's stability in maintaining its optical properties across diverse conditions. In the SM, we noticed that among all the configurations, the optical absorbance is maximized in the 300–450 wavelength range for the CH_2+H+H case, attributed to the bonding between H atoms and the C atom of graphene. In contrast, in the case of GP, CH_2 increases the optical absorbance in the range of 400 to 550 wavelengths due to the system's hybridization and modifying the DOS.

Advancements in 2D materials have expanded the scope of potential applications, particularly in energy harvesting and storage, due to their high electron transport efficiency and extensive surface area with numerous active sites [65]. In this study, a computational approach based on a π-orbital tight-binding Hamiltonian was adopted to simulate the electrical transport phenomena of graphene and GP. The SCC-DFTB method was employed in conjunction with Non-equilibrium Green's functions [59]. In the tight–binding representation, the interaction between atoms is limited to a finite range. The contact self–energy function, also known as the surface Green's function, can be solved for the matrix block corresponding to the atoms near the extended device region using a recursive algorithm [23]. This allows us to accurately describe the electrical transport properties of the materials and analyze their behavior under various conditions. For instance, in studies by M. Mananghaya, electron transport properties of Ag decorated zigzag graphene nanoribbons (Ag/ZGNR) were investigated using non-equilibrium Green's function, where it was observed that the corresponding forward bias voltage across the Ag/ZGNR increases as temperature rises [66]. S. Souma et al. presented a numerical study of the current–voltage characteristics in zigzag–edged graphene nano ribbon (Z–GNR) devices by using the non–equilibrium Green's function in the DFTB method. They demonstrated that the current can be controlled by the additional doping in the channel region [67].

Figure 8 illustrates our findings for graphene in a) and GP in b) that are in good agreement with reported results for pristine graphene in the literature and by Villegas et al. [23] for the pristine GP ribbon; by adding different molecules it is revealed the preferential adsorption of extrinsic chemical species like CH_4, CO_2, and H_2 at interdomain sites, leading to a significant enhancement of scattering effects in both graphene and GP. To delve into this intriguing behavior, the non–pulsating direct current (NPDC) waveform was employed, known for its ability to maintain the stability of adsorbates even under ultrahigh–vacuum conditions. Unlike PDC waves, which exhibit continuous voltage fluctuations, NPDC waves maintain a constant voltage, ensuring the stability of the adsorbed species within the scope of our computational approach. For graphene, it is noteworthy that the adsorption of individual hydrogen, carbon dioxide, and methane molecules leads to a reduction in the transmission probability. This reduction has a direct impact on the density of states within the altered system. Additionally, it is observed that the effects on the DOS of the armchair–wise graphene sheet is associated with the bond formed between carbon atoms and these molecules; which are reflected in the transmission probability of two symmetric minima around the Fermi. On the other hand, when considering the

GP sheet, the presence of singly bonded molecules to carbon atoms does not appear to induce substantial modifications in the transmission probability. However, there is a decrease in the transmission probability within the energy range of approximately ±1.5 to 1.0 eV. This observation highlights the potential of GP as a promising candidate for the development of gas sensors, emphasizing its sensitivity to changes in its surrounding gaseous environment. Since, the strong mechanical properties play a key role in maintaining the structural integrity of porous frameworks, preventing their shrinkage or collapse. Therefore, the presence of channels and pores facilitates rapid electrolyte diffusion, leading to an augmentation in electrical conductivity as shown by our results.

Fig 9 shows the difference of the current for each molecule X as a function of the voltage as:

$$S = 100\% \frac{|I_X - I_g|}{I_X}, \tag{5}$$

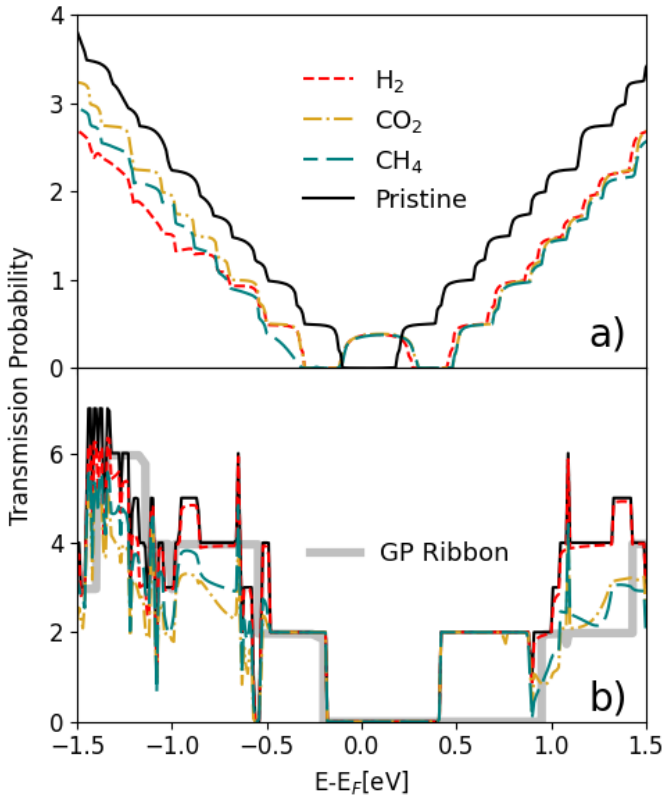

Figure 8: The total transmission probabilities summed over all channels in the nanoribbon graphene direction in a) and through the pores of GP in b) for the pristine surface and with different molecules observed during the bombardment simulations. Reported results for a pristine ribbon [23] are displayed for the GP showing size effects in the band gap value.

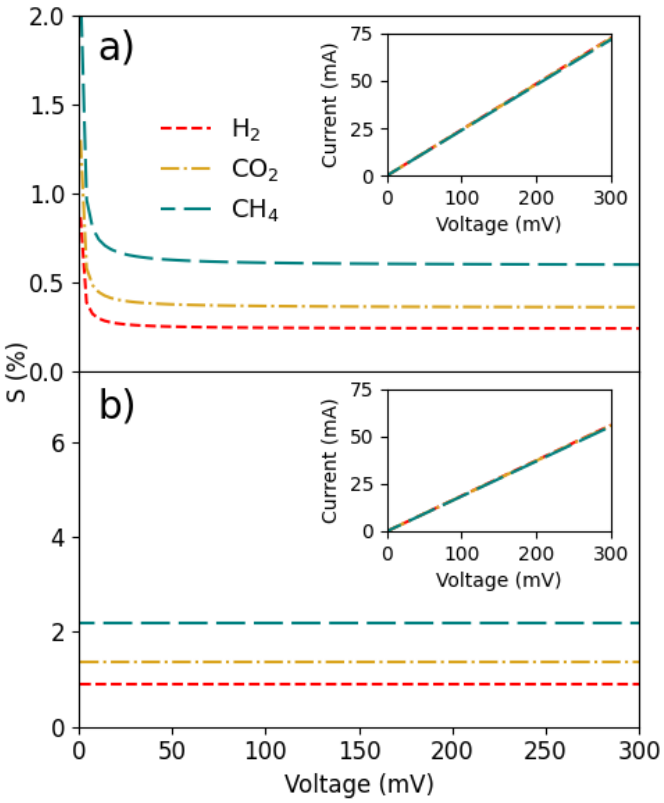

Figure 9: Sensitivity of graphene in a) and graphenelyne in b) considering different molecules and atoms adsorbed. The inset shows the linear current-voltage (I-V) characteristics in the range of 0–300 mV.

with I_X of each molecule and the surface and I_g the current of the graphene in a) and GP in b). Noticing that the adsorption of CH_x compounds increases the sensitivity of the surfaces. The tunneling currents for the sheets as a function of the voltage for various adsorbed molecules are shown in the inset plots by I—U characteristics graphs for voltages below 300 mV. Our results are in a qualititive good agrement with reported experimental data [10] showing a decrease of 25 mV for GP and an efficiency increas of 4% for methane single molecules. Thus, the porous structure of GP offers distinct advantages, including increased surface area, reduced density, and improved accessibility to guest objects. This structure is highly suitable for applications involving light absorption and electron/ion transport. Specifically, it shortens the migration path of charge carriers from the point of generation to the active surface, thereby facilitating electron migration to the surface. Therefore, we suggest that GP based materials can be better candidates than graphene ones for use in field effect tran-

sistors, as Zener diodes, and faster sensors.

4. Conclusion

In this study, we utilize computer simulations to explore the gas separation mechanism and its impact on the optical and electronic properties of graphene and graphenelyne sheets. Our focus is specifically on the emission behavior of CH_4 and CO_2 molecules. To conduct these simulations, we employ a quantum-classical molecular dynamics approach, utilizing the SCC–DFTB method with van der Waals corrections. These corrections are essential to accurately capture the dissociation, chemisorption, and molecule formation processes involved in the dynamics.

We analyze the probabilities of transmission, reflection, and adsorption of the emitted molecules. Our results highlight that GP exhibits significant advantages in gas separation compared to graphene. Specifically, we find that GP enables efficient separation of CO_2 into CO+O and CH_4 into CH_2+H_2 with the highest probabilities to be dissociated. The porosity of GP enhances gas separation rates, facilitates CO_2 purification, and promotes hydrogen production from methane. By conducting electron transport calculations with the non–equilibrium green function method, we noticed that hydrocarbon like CH_2, and CH_4 have the most effects on the electron transport mechanisms for both 2D materials.

Acknowledgements

We acknowledge support from the European Union Horizon 2020 research and innovation program under grant agreement no. 857470 and from the European Regional Development Fund via the Foundation for Polish Science International Research Agenda PLUS program grant No. MAB PLUS/ 2018/8. We acknowledge the computational resources provided by the Interdisciplinary Centre for Mathematical and Computational Modelling (ICM) University of Warsaw under computational allocation no g91–1427 and the CIS High Performance Cluster at the National Centre for Nuclear Research in Poland.

References

[1] E. Ghirardi, G. Brumana, G. Franchini, A. Perdichizzi, H2 contribution to power grid stability in high renewable penetration scenarios, International Journal of Hydrogen Energy 48 (32) (2023) 11956–11969.

[2] Y. Guan, Y. Liu, X. Lin, B. Wang, Q. Lyu, Research progress and perspectives of solid fuels chemical looping reaction with fe-based oxygen carriers, Energy & Fuels 36 (23) (2022) 13956–13984.

[3] Y. Guan, G. Song, C. Li, K. H. Lim, B. Wang, L. Xia, H. Song, Y. Liu, C. Wu, S. Kawi, Ni-based core-shell structured catalysts for efficient conversion of ch4 to h2: A review, Carbon Capture Science Technology 11 (2024) 100200. doi:https://doi.org/10.1016/j.ccst.2024.100200.
URL https://www.sciencedirect.com/science/article/pii/S2772656824000125

[4] I. H. Kadhim, H. A. Hassan, Q. Abdullah, Hydrogen gas sensor based on nanocrystalline sno 2 thin film grown on bare si substrates, Nano-Micro Letters 8 (2016) 20–28.

[5] R. Jana, S. Hajra, P. M. Rajaitha, K. Mistewicz, H. J. Kim, Recent advances in multifunctional materials for gas sensing applications, Journal of Environmental Chemical Engineering 10 (6) (2022) 108543. doi:https://doi.org/10.1016/j.jece.2022.108543.
URL https://www.sciencedirect.com/science/article/pii/S2213343722014166

[6] A. A. Balandin, Thermal properties of graphene and nanostructured carbon materials, Nature materials 10 (8) (2011) 569–581.

[7] B. Wang, Y. Gu, L. Chen, L. Ji, H. Zhu, Q. Sun, Gas sensing devices based on two-dimensional materials: a review, Nanotechnology 33 (25) (2022) 252001.

[8] O. Leenaerts, B. Partoens, F. M. Peeters, Adsorption of h_2O, Nh_3, co, No_2, and no on graphene: A first-principles study, Phys. Rev. B 77 (2008) 125416. doi:10.1103/PhysRevB.77.125416.
URL https://link.aps.org/doi/10.1103/PhysRevB.77.125416

[9] Y. You, J. Deng, X. Tan, N. Gorjizadeh, M. Yoshimura, S. C. Smith, V. Sahajwalla, R. K. Joshi, On the mechanism of gas adsorption for pristine, defective and functionalized graphene, Phys. Chem. Chem. Phys. 19 (2017) 6051–6056.

[10] M. Shaban, S. Ali, M. Rabia, Design and application of nanoporous graphene oxide film for co2, h2, and c2h2 gases sensing, Journal of Materials Research and Technology 8 (5) (2019) 4510–4520. doi:https://doi.org/10.1016/j.jmrt.2019.07.064.
URL https://www.sciencedirect.com/science/article/pii/S223878541831370X

[11] A. Aligayev, F. Raziq, U. Jabbarli, N. Rzayev, L. Qiao, Chapter 17 - morphology and topography of nanotubes, in: Y. Al-Douri (Ed.), Graphene, Nanotubes and Quantum Dots-Based Nanotechnology, Woodhead Publishing Series in Electronic and Optical Materials, Woodhead Publishing, 2022, pp. 355–420. doi:https://doi.org/10.1016/B978-0-323-85457-3.00019-0.
URL https://www.sciencedirect.com/science/article/pii/B9780323854573000190

[12] V. K. Shanmugam, R. A. Mensah, K. Babu, S. Gawusu, A. Chanda, Y. Tu, R. E. Neisiany, M. Försth, G. Sas, O. Das, A review of the synthesis, properties, and applications of 2d materials, Part. Part. Syst. Charact. 39 (2022) 2200031.

[13] F. Gao, R. Menchón, A. Garcia-Lekue, et al., Tunable spin and conductance in porphyrin-graphene nanoribbon

hybrids, Communications Physics 6 (2023) 115.
[14] A. Hirsch, The era of carbon allotropes, Nature materials 9 (11) (2010) 868–871.
[15] H. R. Karfunkel, T. Dressler, New hypothetical carbon allotropes of remarkable stability estimated by mndo solid-state scf computations, Journal of the American Chemical Society 114 (7) (1992) 2285–2288.
[16] R. Baughman, H. Eckhardt, M. Kertesz, Structure-property predictions for new planar forms of carbon: Layered phases containing sp 2 and sp atoms, The Journal of chemical physics 87 (11) (1987) 6687–6699.
[17] Q. Li, Y. Ma, A. R. Oganov, H. Wang, H. Wang, Y. Xu, T. Cui, H.-K. Mao, G. Zou, Superhard monoclinic polymorph of carbon, Physical review letters 102 (17) (2009) 175506.
[18] X.-L. Sheng, Q.-B. Yan, F. Ye, Q.-R. Zheng, G. Su, T-carbon: a novel carbon allotrope, Physical review letters 106 (15) (2011) 155703.
[19] G. Lee, G. Yang, A. Cho, J. W. Han, J. Kim, Defect-engineered graphene chemical sensors with ultrahigh sensitivity, Phys. Chem. Chem. Phys. 18 (2016) 14198–14204.
[20] A. Balaban, C. C. Rentia, E. Ciupitu, Chemical graphs. 6. estimation of relative stability of several planar and tridimensional lattices for elementary carbon, Revue Roumaine de Chimie 13 (2) (1968) 231–+.
[21] A. Balaban, D. Klein, C. Folden, Diamond-graphite hybrids, Chemical Physics Letters 217 (3) (1994) 266–270.
[22] Q. Song, B. Wang, K. Deng, X. Feng, M. Wagner, J. D. Gale, K. MĂĽllen, L. Zhi, Graphenylene, a unique two-dimensional carbon network with nondelocalized cyclohexatriene units, J. Mater. Chem. C 1 (2013) 38–41.
[23] L. Villegas-Lelovsky, R. Paupitz, Graphenylene-based nanoribbons for novel molecular electronic devices, Phys. Chem. Chem. Phys. 22 (2020) 28365–28375. doi:10.1039/D0CP04188B.
URL http://dx.doi.org/10.1039/D0CP04188B
[24] Q. Du, P. Tang, H. Huang, et al., A new type of two-dimensional carbon crystal prepared from 1,3,5-trihydroxybenzene, Scientific Reports 7 (2017) 40796.
[25] R. Zhang, J. Jiang, The art of designing carbon allotropes, Frontiers in Physics 14 (2019) 13401. doi:10.1007/s11467-018-0836-5.
[26] G. Brunetto, P. Autreto, L. Machado, B. Santos, R. P. Dos Santos, D. S. Galvao, Nonzero gap two-dimensional carbon allotrope from porous graphene, The Journal of Physical Chemistry C 116 (23) (2012) 12810–12813.
[27] A. Kochaev, R. Meftakhutdinov, R. Sibatov, D. Timkaeva, Optical and thermoelectric properties of graphenylene and octagraphene nanotubes from first-principles calculations, Computational Materials Science 186 (2021) 109999. doi:https://doi.org/10.1016/j.commatsci.2020.109999.
URL https://www.sciencedirect.com/science/article/pii/S0927025620304900
[28] N. F. Martins, G. S. L. Fabris, A. R. Albuquerque, R. Paupitz, J. R. Sambrano, Graphenylene-Like Structures as a New Class of Multifunctional Materials Alternatives to Graphene, Springer International Publishing, Cham, 2022, pp. 209–230.
[29] S. J. Mahdizadeh, E. K. Goharshadi, Multicomponent gas separation and purification using advanced 2d carbonaceous nanomaterials, RSC Adv. 10 (2020) 24255–24264.
[30] J. Xu, S. Zhou, P. Sang, J. Li, L. Zhao, Inorganic graphenylene as a promising novel boron nitrogen membrane for hydrogen purification: a computational study, Journal of Materials Science 52 (17) (2017) 10285–10293.
[31] L. Zhu, Y. Jin, Q. Xue, X. Li, H. Zheng, T. Wu, C. Ling, Theoretical study of a tunable and strain-controlled nanoporous graphenylene membrane for multifunctional gas separation, Journal of Materials Chemistry A 4 (39) (2016) 15015–15021.
[32] P. Rezaee, H. R. Naeij, Graphenylene–1 membrane: An excellent candidate for hydrogen purification and helium separation, Carbon 157 (2020) 779–787.
[33] M. S. Motallebipour, J. Karimi-Sabet, Graphenylene and inorganic graphenylene nanopores for gas-phase 4 he/3 he separation: kinetic and steady-state considerations, Physical Chemistry Chemical Physics 23 (27) (2021) 14706–14715.
[34] G. S. Fabris, N. L. Marana, J. A. Laranjeira, E. Longo, J. R. Sambrano, New two-dimensional zinc oxide nanosheets: Properties, stability, and interconversion, Materials Letters 275 (2020) 128067. doi:https://doi.org/10.1016/j.matlet.2020.128067.
URL https://www.sciencedirect.com/science/article/pii/S0167577X20307722
[35] J. A. Laranjeira, J. F. Silva, P. A. Denis, A. S. Maia, J. R. Sambrano, Novel buckled graphenylene-like inn and its strain engineering effects, Computational and Theoretical Chemistry 1231 (2024) 114418. doi:https://doi.org/10.1016/j.comptc.2023.114418.
URL https://www.sciencedirect.com/science/article/pii/S2210271X23004000
[36] N. F. Martins, J. A. Laranjeira, S. A. Azevedo, G. S. Fabris, J. R. Sambrano, Structural, electronic and mechanical properties of a novel graphenylene-like structure based on gec, Journal of Physics and Chemistry of Solids 181 (2023) 111518. doi:https://doi.org/10.1016/j.jpcs.2023.111518.
URL https://www.sciencedirect.com/science/article/pii/S0022369723003086
[37] J. A. Laranjeira, N. F. Martins, P. A. Denis, J. R. Sambrano, Graphenyldiene: A new sp2-graphene-like nanosheet, Carbon Trends 14 (2024) 100321. doi:https://doi.org/10.1016/j.cartre.2024.100321.
URL https://www.sciencedirect.com/science/article/pii/S2667056924000026
[38] E. Perim, R. Paupitz, P. Autreto, D. Galvao, Inorganic graphenylene: a porous two-dimensional material with tunable band gap, The Journal of Physical Chemistry C 118 (41) (2014) 23670–23674.
[39] G. S. Fabris, N. L. Marana, J. A. Laranjeira, E. Longo, J. R. Sambrano, New two-dimensional zinc oxide nanosheets: Properties, stability, and interconversion, Materials Letters 275 (2020) 128067.
[40] G. S. Fabris, C. A. Paskocimas, J. R. Sambrano, R. Paupitz, One-and two-dimensional structures based on gallium nitride, Journal of Solid State Chemistry 303 (2021) 122513.
[41] N. F. Martins, G. S. Fabris, A. R. Albuquerque, J. R. Sambrano, A new multifunctional two-dimensional monolayer based on silicon carbide, FlatChem 30 (2021) 100286.
[42] V. K. Sangwan, M. C. Hersam, Electronic transport in two-dimensional materials, Annual Review of Physical Chemistry 69 (1) (2018) 299–325.

[43] J. Zhang, L. Liu, Y. Yang, Q. Huang, D. Li, D. Zeng, A review on two-dimensional materials for chemiresistive- and fet-type gas sensors, Phys. Chem. Chem. Phys. 23 (2021) 15420–15439.

[44] W.-T. Chung, I. M. Mekhemer, M. G. Mohamed, A. M. Elewa, A. F. EL-Mahdy, H.-H. Chou, S.-W. Kuo, K. C.-W. Wu, Recent advances in metal/covalent organic frameworks based materials: Their synthesis, structure design and potential applications for hydrogen production, Coordination Chemistry Reviews 483 (2023) 215066. doi:https://doi.org/10.1016/j.ccr.2023.215066.
URL https://www.sciencedirect.com/science/article/pii/S0010854523000553

[45] Z. Wang, X.-F. Zhou, X. Zhang, Q. Zhu, H. Dong, M. Zhao, A. R. Oganov, Phagraphene: A low-energy graphene allotrope composed of 5â€“6â€“7 carbon rings with distorted dirac cones, Nano Letters 15 (9) (2015) 6182–6186.

[46] J. Whitener, Keith E., Review Article: Hydrogenated graphene: A userâ€™s guide, Journal of Vacuum Science & Technology A 36 (5) (2018) 05G401.

[47] B. Hourahine, B. Aradi, V. Blum, F. Bonafe, et al., DFTB+, a software package for efficient approximate density functional theory based atomistic simulations, The Journal of Chemical Physics 152 (12) (2020) 124101.

[48] Q. Cui, M. Elstner, E. Kaxiras, T. Frauenheim, M. Karplus, A qm/mm implementation of the self-consistent charge density functional tight binding (scc-dftb) method, The Journal of Physical Chemistry B 105 (2) (2001) 569–585. doi:10.1021/jp0029109.

[49] E. Santos, W. Schmickler, Hydrogen adsorption on doped graphene investigated by a dft-based tight-binding method, Journal of Physics: Condensed Matter 33 (50) (2021) 504001. doi:10.1088/1361-648X/ac28c0.
URL https://dx.doi.org/10.1088/1361-648X/ac28c0

[50] S. Arunragsa, Y. Seekaew, W. Pon-On, C. Wongchoosuk, Hydroxyl edge-functionalized graphene quantum dots for gas-sensing applications, Diamond and Related Materials 105 (2020) 107790. doi:https://doi.org/10.1016/j.diamond.2020.107790.
URL https://www.sciencedirect.com/science/article/pii/S0925963520300674

[51] G. Fabris, N. Marana, E. Longo, J. Sambrano, Theoretical study of porous surfaces derived from graphene and boron nitride, Journal of Solid State Chemistry 258 (2018) 247–255.

[52] K. J. Miller, Additivity methods in molecular polarizability, Journal of the American Chemical Society 112 (23) (1990) 8533–8542.

[53] M. Elstner, P. Hobza, T. Frauenheim, S. Suhai, E. Kaxiras, Hydrogen bonding and stacking interactions of nucleic acid base pairs: A density-functional-theory based treatment, The Journal of Chemical Physics 114 (12) (2001) 5149–5155.

[54] F. J. Dominguez-Gutierrez, P. S. Krstic, S. Irle, R. Cabrera-Trujillo, Low-energy hydrogen uptake by small-cage cn and cn-1b fullerenes, Carbon 134 (2018) 189–198.

[55] M. Novotny, F. J. Dominguez-Gutierrez, P. Krstic, A computational study of hydrogen detection by borophene, J. Mater. Chem. C 5 (2017) 5426–5433.

[56] F. J. Dominguez-Gutierrez, A. Aligayev, W. Huo, M. Chourashiya, Q. Xu, S. Papanikolaou, Dynamical pathways for the interaction of o2, h2o, ch4, and co2 with Î±-alumina surfaces: Density-functional tight-binding calculations, physica status solidi (b) n/a (n/a) 2200567.

[57] D. M. Marquez, C. G. SÃˇnchez, Quantum efficiency of the photo-induced electronic transfer in dyeâ€“tio2 complexes, Phys. Chem. Chem. Phys. 20 (2018) 26280–26287.

[58] M. B. Oviedo, C. F. A. Negre, C. G. SÃˇnchez, Dynamical simulation of the optical response of photosynthetic pigments, Phys. Chem. Chem. Phys. 12 (2010) 6706–6711.

[59] A. Pecchia, G. Penazzi, L. Salvucci, A. D. Carlo, Non-equilibrium green's functions in density functional tight binding: method and applications, New Journal of Physics 10 (6) (2008) 065022. doi:10.1088/1367-2630/10/6/065022.
URL https://dx.doi.org/10.1088/1367-2630/10/6/065022

[60] G. Lee, I. Hong, J. Ahn, H. Shin, A. Benali, Y. Kwon, Hydrogen separation with a graphenylene monolayer: Diffusion Monte Carlo study, The Journal of Chemical Physics 157 (14) (2022) 144703.

[61] C. Lee, N. Leconte, J. Kim, D. Cho, I.-W. Lyo, E. Choi, Optical spectroscopy study on the effect of hydrogen adsorption on graphene, Carbon 103 (2016) 109–114. doi:https://doi.org/10.1016/j.carbon.2016.03.008.
URL https://www.sciencedirect.com/science/article/pii/S000862231630197X

[62] W. Zhang, W.-C. Lu, H.-X. Zhang, K. Ho, C. Wang, Hydrogen adatom interaction on graphene: A first principles study, Carbon 131 (2018) 137–141. doi:https://doi.org/10.1016/j.carbon.2018.01.096.
URL https://www.sciencedirect.com/science/article/pii/S0008622318301052

[63] Y. Gui, X. Peng, K. Liu, Z. Ding, Adsorption of c2h2, ch4 and co on mn-doped graphene: Atomic, electronic, and gas-sensing properties, Physica E: Low-dimensional Systems and Nanostructures 119 (2020) 113959. doi:https://doi.org/10.1016/j.physe.2020.113959.
URL https://www.sciencedirect.com/science/article/pii/S1386947719313116

[64] M. Hashemi, M. H. Farzad, N. A. Mortensen, S. Xiao, Enhanced absorption of graphene in the visible region by use of plasmonic nanostructures, Journal of Optics 15 (5) (2013) 055003. doi:10.1088/2040-8978/15/5/055003.
URL https://dx.doi.org/10.1088/2040-8978/15/5/055003

[65] M. R. Kumar, S. Singh, H. M. Fahmy, N. K. Jaiswal, S. Akin, A. E. Shalan, S. Lanceros-Mendez, M. Salado, Next generation 2d materials for anodes in battery applications, Journal of Power Sources 556 (2023) 232256. doi:https://doi.org/10.1016/j.jpowsour.2022.232256.
URL https://www.sciencedirect.com/science/article/pii/S0378775322012332

[66] M. Mananghaya, Transport properties of ag decorated zigzag graphene nanoribbons as a function of temperature: a density functional based tight binding molecular dynamics study, Adsorption 25 (2019) 1655–1662.

[67] S. Souma, M. Ogawa, T. Yamamoto, K. Watanabe, Numerical simulation of electronic transport in zigzag-edged graphene nano-ribbon devices, Journal of Computational Electronics 7 (2008) 390–393.